Received: 26 February 2022 | Revised: 6 October 2022 | Accepted: 5 December 2022

DOI: 10.1002/mma.8963

RESEARCH ARTICLE

WILEY

Improved accuracy and convergence of homotopy-based solutions for aggregation–fragmentation models

Prakrati Kushwah | **Jitraj Saha**

Department of Mathematics, National Institute of Technology Tiruchirappalli, Tiruchirappalli, Tamil Nadu, 620015, India

Correspondence
Jitraj Saha, Department of Mathematics, National Institute of Technology Tiruchirappalli, Tamil Nadu, 620015, India.
Email: jitraj@nitt.edu

Communicated by: M. Brokate

Funding information
PK thanks Ministry of Education (MoE), Government of India, for their funding support during her PhD program. JS thanks NITT for their support through seed grant (file no.: NITT / R & C / SEED GRANT / 19 - 20 / P - 13 / MATHS / JS / E1) during this work.

We discuss the formulation of a numerical scheme based on the homotopy method to solve different aggregation–fragmentation models including the simultaneous event. Several test cases are considered and analyzed qualitatively and quantitatively to ascertain the improved accuracy and efficiency of the proposed model over the existing semi-analytical models. The generalized solution of the truncated problem is obtained for some test cases, which in the limiting sense tends to the exact solution. A detailed convergence analysis of the scheme is also studied.

KEYWORDS

aggregation–fragmentation equation, convergence, mass conservation, gelation, homotopy analysis method

MSC CLASSIFICATION

Primary 34A12, 35Q70, 45K05, Secondary 47J35

1 | INTRODUCTION

The interactions among the particles in a dynamical system lead towards the change in their different physical properties like mass, shape, size, and so on. These phenomena are well-known as *particulate events*. The application of particulate events can be found widely, ranging from the natural phenomena to different controlled laboratory/manufacturing units. For instance, the formation of stars and planets,[1,2] merging of rain droplets,[3,4] formation of gas bubbles during the eruption of lava/magma,[5,6] migrating barchan dunes on Mars and Earth (aeolian geomorphology),[7,8] and so on are different natural particulate events. Whereas different chemical engineering and related colloidal industries like manufacturing of tablets in pharmaceutical sector,[9,10] food processing industries (like whey, powdered milk, coffee, etc.),[11–13] in fluidized bed granulator,[14,15] and so on deal with the application of different particulate events. During particulate events, when two particles join to form a larger cluster, it is called *aggregation*. On the other hand, the breakage of a particle into smaller pieces is coined as *fragmentation*. It is obvious that the particulate events result in the evolution of particle size distribution, as well as their number with respect to time. In this regard, the aggregation results in the decrease of the total number of particles, and fragmentation leads to the increase of the number. To capture all these phenomena, a mathematical model called *population balance equations* (PBEs) is used. In general, PBEs are integro-partial differential equations supported by some initial data.

1.1 | General aggregation–fragmentation (AF) equation

Consider a system undergoing particulate process, and $n(t, x)$ denotes the number density of particles of size x at time t. Then for $x \geq 0$ and $0 \leq t \leq T < \infty$, the *simultaneous AF* equation is written as follows[16]:

$$\frac{\partial n(t,x)}{\partial t} = \frac{1}{2}\int_0^x \beta(x-\epsilon,\epsilon)n(t,x-\epsilon)n(t,\epsilon)\mathrm{d}\epsilon - n(t,x)\int_0^\infty \beta(x,\epsilon)n(t,\epsilon)\mathrm{d}\epsilon + \int_x^\infty b(x|y)s(y)n(t,y)\mathrm{d}y - s(x)n(t,x), \tag{1.1}$$

along with the initial condition

$$n(0,x) \geq 0, \text{ for all } x \geq 0. \tag{1.2}$$

The left-hand side (lhs) of the initial value problem (1.1) denotes the time evolution of particle number density $n(t,x)$. The function $\beta(x,\epsilon)$ appearing in the first two terms in the right-hand side (rhs) is called the aggregation kernel and denotes the rate at which particles of size x and size ϵ merge to form a larger cluster of size $(x+\epsilon)$. In general, $\beta(x,\epsilon)$ is considered to be symmetric and nonnegative function of x and ϵ. The last two terms contain the selection function $s(y)$ which describes the rate at which particles of size y are selected to break. The function $b(x|y)$ appearing only in the third term represents the distribution of daughter particles of size x formed due to the breakage of a larger particle of size y. In general, both s and b are nonnegative functions of their arguments.

Additionally, the breakage function b is assumed to satisfy the following properties

$$b(x|y) = 0 \text{ for all } x \geq y, \quad \int_0^y xb(x|y)\mathrm{d}x = y \text{ and } \int_0^y b(x|y)\mathrm{d}x = \nu(\geq 2). \tag{1.3}$$

Here, the first relation is a trivial property. The second relation defines that the sum of the sizes of all the daughter particles is equal to the size of the mother particle, and the last one defines that ν number of fragments are produced when y undergoes fragmentation. The assumption $\nu \geq 2$ defines a multifragmentation model; that is, more than two fragments are allowed to produce during fragmentation.

To this end, recalling Equation (1.1) each of the first and the third terms is called *birth term*, because they result towards the inclusion of particle of size x in the system. Hence, they are associated with a positive sign. On the other hand, the second and the third terms define the removal of the particle size x from the system and hence called *death terms*. The factor 1/2 present in the first term is used to balance the double counting of the particles formed.

For the PBEs, the moment function of the number density $n(t,x)$ is defined as follows:

$$\mu_i(t) = \int_0^\infty x^i n(t,x)\mathrm{d}x, \text{ for } i = 0,1,2,\ldots, \tag{1.4}$$

and they play significant roles to represent various physical entities. For example, the zeroth moment $\mu_0(t)$ defines the total number of particles in the system, the first moment $\mu_1(t)$ represents the total mass of the particulate system, and so on.

In general, no mass can be created or destroyed; therefore, all phenomena are expected to abide by the mass conservation laws, which is mathematically expressed as follows:

$$\int_0^\infty xn(t,x)\mathrm{d}x = \int_0^\infty xn(0,x)\mathrm{d}x. \tag{1.5}$$

1.2 | Literature review and motivation

The onset of high-speed computing has facilitate many researchers to work on the solutions of different types of PBEs as they bear significant responsibilities in different manufacturing units as well as in CFD-simulations.[17–23] However, the complicated nature of the PBE models has rendered the search for exact solutions within a few number of simple kernels.[24–26] Therefore, numerical methods are required to solve the PBEs. In this context, schemes based on sectional discretizations,[27–29] methods of moments,[30–32] population dynamics algorithms,[33,34] semi-analytical methods,[35,36] and so on are used considerably to solve different problems with empirical kernels. In early 2000, two homotopy-based methods, namely, the *homotopy perturbation method* (HPM)[37] and the *homotopy analysis method* (HAM),[38] were introduced to solve different real-life problems. Over the years, these homotopy-based methods have gained popularity due to their ability to solve different complicated problems. One major advantage of these methods over the conventional numerical

methods is that they find the solutions in the form of an infinite series. Therefore, knowing a few terms and then passing the limits to infinity lead us towards the exact solutions of the considered problem. In several occasions, it is observed that due to the presence of a number of free-to-choose parameters, HAM exhibits better robustness over HPM to predict the solutions.[39] In other words, for same number of terms, the HAM-based series solutions generate highly accurate solutions as compared with HPM-based series solutions. This has a major advantage to reduce the computational cost considerably.

Several articles on different numerical models to solve PBEs are available in the literature; however, the search for solutions by semi-analytical methods has not been explored much. In the recent articles,[35,36] the authors have applied Adomian decomposition method (ADM) and HPM, respectively, to obtain solutions for different PBEs and also studied their convergence. It should be noted that ADM is basically a particular case of HAM for certain choices of the free-to-choose parameters (details are given in the subsequent discussion). Note that the *efficiency* of a method for solving PBEs is defined upon the accuracy to predict the number density function, as well as various significant moment functions. In this context, an efficient series-based semi-analytical model should be stable enough to produce accurate solutions of the above properties by considering only a few terms in their series representation.

To this end, this work is the first evidence where HAM is designed to define a recursive scheme for solving PBEs in different forms, namely, (i) pure fragmentation, (ii) pure aggregation, and (iii) simultaneous AF models. In this work, we propose to solve the PBEs with HAM and compare the efficiency over HPM by considering several test problems. Note that pure fragmentation equation is linear in $n(t,x)$, and two test cases with linear and quadratic selection functions are taken into consideration. For quadratic selection, function particles break at higher rate as compared with the linear one. Here, we are able to introduce the HAM-based solution in closed form for the first time in literature. The next two problems are considered for nonlinear aggregation model with sum and product kernels. The total particle mass is conserved in the system throughout the entire time evolution for sum kernel. However, for product kernel, system starts loosing the mass after finite time. In other words, a cluster of large size forms and gets eliminated from the system. We therefore examined aggregation event with product kernel in order to confirm this intriguing phenomenon. In many real-life scenarios, fragmentation and aggregation take place simultaneously. Thus, we took into account the simultaneous AF equation in the last problem. Due to the combination of linear and nonlinear equations, finding the solution becomes more challenging. For this case, constant aggregation rate and binary breakup with linear selection function is considered. The solution for this case depends on a parameter, which can determine whether the process will be dominated by aggregation or fragmentation. We have considered both the cases and discussed them in detail. The error analysis is performed both qualitatively and quantitatively for all the test problems. In this regard, the previous article[36] solves some sample problems on pure fragmentation and pure aggregation using HPM. However, authors have not obtained HPM-based solution for simultaneous AF equation. Therefore, we have also obtained the HPM-based series solution for the first time to compare the efficiency of HAM-based series solution.

The article is organized as follows: In the subsequent section, we discuss the preliminary ideas on HAM and also present the recursive schemes corresponding to different PBEs. In Section 2.3, the convergence analysis of the HAM-based recursive schemes is also proved. Section 3 is devoted on the detailed discussions of several sample problems. Finally, we present some concluding remarks in Section 4.

2 | DISCRETE FORMULATIONS

2.1 | Preliminaries

The HAM is basically a recursive scheme for which the initial guess v_0 of the solution $n(t,x)$ should be known. In general, the initial guess of the solution is considered to coincide with the initial data, that is,

$$v_0(t,x) = n(0,x). \tag{2.1}$$

Further, let $q \in [0,1]$ denote the embedding parameter. The primary idea of the HAM is to construct a continuous mapping $n(t,x) \mapsto v(t,x;q)$ through a homotopy function $\mathscr{H}$, where

$$\mathscr{H}[v(t,x;q);q,\hbar,H] := (1-q)\mathscr{L}[v(t,x;q) - v_0(t,x)] - q\hbar H(t,x)\mathscr{N}[v(t,x;q)] = 0, \tag{2.2}$$

in such a way that as the embedding parameter q varies from 0 to 1, the homotopy-based solution $v(t,x;q)$ varies from the initial guess v_0 to the exact solution $n(t,x)$. Here in Equation (2.2), $\mathscr{L}$ defines a linear operator, $\mathscr{N}$ is the generalized

operator (defined according to the problem), $\hbar$ is an auxiliary parameter, and $H(t,x)$ is an auxiliary function. Based upon our problem, the linear operator is chosen as follows:

$$\mathscr{L}\left[v(t,x;q)\right] = \frac{\partial v(t,x;q)}{\partial t} \text{ such that } \mathscr{L}\left[f(x,y)\right] = 0 \iff f(x,y) = 0. \tag{2.3}$$

Let us consider the generalized problem in the following operator form

$$\mathscr{N}\left[n(t,x)\right] = 0. \tag{2.4}$$

For $q = 0$, Equation (2.2) along with (2.3) gives

$$\mathscr{L}\left[v(t,x;0) - v_0(t,x)\right] = 0 \text{ implies } v(t,x;0) = v_0(t,x). \tag{2.5}$$

Again for $q = 1$, under the consideration that $\hbar \neq 0$ and $H(t,x) \neq 0$, relation (2.2) becomes

$$\mathscr{N}\left[v(t,x;1)\right] = 0, \tag{2.6}$$

which replicates the original problem (2.4), provided

$$v(t,x;1) = n(t,x). \tag{2.7}$$

Hence, according to the construction of Equations (2.5) and (2.7), the homotopy-based solution $v(t,x;q)$ varies from the initial guess $v_0(t,x)$ to the exact solution $n(t,x)$ as the embedding parameter q varies from 0 to 1. In this regard, Equation (2.2) is called *zero-order deformation equation*.

The freedom to choose $\mathscr{L}, n_0(t,x), \hbar, H(t,x)$ enables us to adjust all the parameters properly such that the solution of deformation equation exists for $q \in [0,1]$. Consider that $v(t,x;q)$ is sufficiently smooth with respect to embedding parameter q, then the mth-order derivative of $v(t,x;q)$ with respect to q is defined as follows:

$$v_m(t,x) := \frac{v_0^{[m]}(t,x)}{m!} = \frac{1}{m!}\frac{\partial^m v(t,x;q)}{\partial q^m}\bigg|_{q=0}. \tag{2.8}$$

By Taylor's theorem, $v(t,x;q)$ can be expanded in a power series of q as follows:

$$v(t,x;q) = v(t,x;0) + \sum_{m=1}^{\infty}\frac{v_0^m(t,x)}{m!}q^m = v_0(t,x) + \sum_{m=1}^{\infty} v_m(t,x)q^m. \tag{2.9}$$

In general, the above series will converge for $q = 1$, and hence using relation (2.6) we have

$$n(t,x) = v_0(t,x) + \sum_{m=1}^{\infty} v_m(t,x). \tag{2.10}$$

We define the vector $\vec{v}_m := \{v_0(t,x), v_1(t,x), v_2(t,x), \ldots, v_m(t,x)\}$. Differentiating the zero-order deformation Equation (2.2) m-times with respect to q then dividing it by $m!$ and finally setting $q = 0$, we get the following mth-order deformation equation

$$\mathscr{L}\left[v_m(t,x) - \chi_m v_{m-1}(t,x)\right] = \hbar H(t,x)\mathcal{R}_m(\vec{v}_{m-1}, t, x) \tag{2.11}$$

with initial condition $v_m(0,x) = 0$, where $\chi_m := \begin{cases} 0, & \text{when } m \leq 1, \\ 1, & \text{when } m > 1, \end{cases}$

and

$$\mathcal{R}_m(\vec{v}_{m-1},t,x)=\frac{1}{(m-1)!}\frac{\partial^{m-1}\mathcal{N}\left[v(t,x;q)\right]}{\partial q^{m-1}}\bigg|_{q=0}=\frac{1}{(m-1)!}\frac{\partial^{m-1}}{\partial q^{m-1}}\mathcal{N}\left[\sum_{j=0}^{\infty}v_j(t,x)q^j\right]_{q=0}. \tag{2.12}$$

Thus, the solution of Equation (2.11) is given by

$$v_m(t,x)=\chi_m v_{m-1}(t,x)+\int_0^t \hbar H(t,s)\mathcal{R}_m\left(\vec{v}_{m-1},s,x\right)\mathrm{d}s, \tag{2.13}$$

where $\mathcal{R}_m$ is given by formulation (2.12). In accordance with the solution (2.10), the mth-order approximation of $n(t,x)$ is given by

$$n(t,x)\approx\sum_{j=0}^{m}v_m(t,x)=:\hat{v}^{[m]}(t,x)\ \text{(say)}. \tag{2.14}$$

In the subsequent discussion, we derive the homotopy-based recursive scheme for the pure fragmentation, pure aggregation, and simultaneous AF problems. The convergence criterion of the new recursive schemes is also studied in due course.

2.2 | Recursive scheme for the AF models

In light of the above discussion, we recall the simultaneous AF Equation (1.1) to define the generalized operator $\mathcal{N}$ by

$$\begin{aligned}\mathcal{N}\left[n(t,x)\right]:=&\frac{\partial n(t,x)}{\partial t}-\frac{1}{2}\int_0^x\beta(x-\epsilon,\epsilon)n(t,x-\epsilon)n(t,\epsilon)\mathrm{d}\epsilon+n(t,x)\int_0^\infty\beta(x,\epsilon)n(t,\epsilon)\mathrm{d}\epsilon\\&-\int_x^\infty b(x|y)s(y)n(t,y)\mathrm{d}y+s(x)n(t,x)=0.\end{aligned}$$

The HAM-based recursive solution $v_m(t,x)$ is obtained from Equation (2.13), where $\mathcal{R}_m$ is given by

$$\begin{aligned}\mathcal{R}_m\left(\vec{v}_{m-1},t,x\right)=&\frac{\partial v_{m-1}(t,x)}{\partial t}-\frac{1}{2}\int_0^x\beta(x-\epsilon,\epsilon)\sum_{i=0}^{m-1}v_i(t,x-\epsilon)v_{m-1-i}(t,\epsilon)\mathrm{d}\epsilon\\&+\sum_{i=0}^{m-1}v_i(t,x)\int_0^\infty\beta(x,\epsilon)v_{m-1-i}(t,\epsilon)\mathrm{d}\epsilon\\&-\int_x^\infty b(x|y)s(y)v_{m-1}(t,x)\mathrm{d}y+s(x)v_{m-1}(t,x).\end{aligned} \tag{2.15}$$

Further simplification of $\mathcal{R}_m$ is obtained in Section 3, under the different choices of the kernels $\beta(x,\epsilon)$, $s(x)$, and $b(x|y)$. Note that the pure fragmentation and pure aggregation models are obtained by setting $\beta=0$ and $s=0$, respectively, in Equation (1.1).

To this end, the HAM-based recursive solution (2.13) for the pure fragmentation is obtained by setting $\beta=0$ in the definition of $\mathcal{R}_m$ (2.15) which reads as

$$\mathcal{R}_m\left(\vec{v}_{m-1},t,x\right)=\frac{\partial v_{m-1}(t,x)}{\partial t}-\int_x^\infty b(x|y)s(y)v_{m-1}(t,x)\mathrm{d}y+s(x)v_{m-1}(t,x). \tag{2.16}$$

Similarly, setting $s=0$ in relation (2.15) defines the $\mathcal{R}_m$ corresponding to the pure aggregation equation as

$$\begin{aligned}\mathcal{R}_m\left(\vec{v}_{m-1},t,x\right)=&\frac{\partial v_{m-1}(t,x)}{\partial t}-\frac{1}{2}\int_0^x\beta(x-\epsilon,\epsilon)\sum_{i=0}^{m-1}v_i(t,x-\epsilon)v_{m-1-i}(t,\epsilon)\mathrm{d}\epsilon\\&+\sum_{i=0}^{m-1}v_i(t,x)\int_0^\infty\beta(x,\epsilon)v_{m-1-i}(t,\epsilon)\mathrm{d}\epsilon.\end{aligned} \tag{2.17}$$

Remark 2.1. One can generate the ADM-based recursive scheme by setting $H(t,x) = 1$ and $\hbar = -1$ in the Equation (2.13). The design of HAM suggests that $\hbar$ plays a pivotal role to improve the efficiency of the method. The subsequent section validates that a good choice of $\hbar$, instead of a fixed value, improves the efficiency of the HAM-based solutions.

2.3 | Convergence theorem

In this part, we state and prove the convergence criterion of the recursive solutions $v_m(t,x)$ generated with the help of the formulation (2.13). Since model (2.13) along with the $\mathcal{R}_m$ (2.15) represents the generalized AF model, therefore, we analyze the convergence of the solution with $\mathcal{R}_m$ given by (2.15). Other two models of pure fragmentation and pure aggregation with $\mathcal{R}_m$'s given by (2.16) and (2.17), respectively, being the particular cases of the above considered problem.

Theorem 2.1. *If the recursive solution $v_m(t,x)$ is governed by the higher-order deformation Equation (2.11) with $\mathcal{R}_m$ given by (2.15) and under the initial condition (2.1), then as long as the series (2.9) converges, it must be the exact solution of problem (2.4).*

Proof. Consider that the series $\sum_{m=0}^{\infty} v_m(t,x)$ converges. Then we can write

$$n(t,x) = \sum_{m=0}^{\infty} v_m(t,x), \text{ which implies } \lim_{m\to\infty} v_m(t,x) = 0. \tag{2.18}$$

In this context,

$$\sum_{m=0}^{j} \left[v_m(t,x) - \chi_m v_{m-1}(t,x)\right] = v_1 + (v_2 - v_1) + \ \dots \ + \left(v_j - v_{j-1}\right) = v_j(t,x),$$

and hence, in accordance with relation (2.18), we get

$$\sum_{m=0}^{\infty} \left[v_m(t,x) - \chi_m v_{m-1}(t,x)\right] = \lim_{j\to\infty} v_j(t,x) = 0.$$

Due to the linearity property of $\mathscr{L}$, we have

$$\sum_{m=0}^{\infty} \mathscr{L}\left[v_m(t,x) - \chi_m v_{m-1}(t,x)\right] = \mathscr{L} \sum_{m=0}^{\infty} \left[v_m(t,x) - \chi_m v_{m-1}(t,x)\right] = 0.$$

Thus, recalling mth-order deformation equation, we obtain

$$\sum_{m=0}^{\infty} \mathscr{L}\left[v_m(t,x) - \chi_m v_{m-1}(t,x)\right] = \hbar H(t,x) \sum_{m=1}^{\infty} \mathcal{R}_m\left[\vec{v}_{m-1}\right] = 0.$$

Since $\hbar \neq 0$ and $H(t,x) \neq 0$, therefore,

$$\sum_{m=1}^{\infty} \mathcal{R}_m\left[\vec{v}_{m-1}\right] = 0. \tag{2.19}$$

Recalling (2.15), we get

$$\begin{aligned}\sum_{m=1}^{\infty}\mathcal{R}_m\left[\vec{v}_{m-1}\right] &= \sum_{m=1}^{\infty}\left[\frac{\partial v_{m-1}(t,x)}{\partial t} - \frac{1}{2}\int_0^x \beta(x-\epsilon,\epsilon)\sum_{i=0}^{m-1} v_i(t,x-\epsilon)v_{m-1-i}(t,\epsilon)\mathrm{d}\epsilon\right.\\ &\quad + \sum_{i=0}^{m-1} v_i(t,x)\int_0^{\infty}\beta(x,\epsilon)v_{m-1-i}(t,\epsilon)\mathrm{d}\epsilon\\ &\quad \left. - \int_x^{\infty} b(x|y)s(y)v_{m-1}(t,x)\mathrm{d}y + s(x)v_{m-1}(t,x)\right]\\ &= \sum_{m=1}^{\infty}\frac{\partial v_{m-1}(t,x)}{\partial t} - \frac{1}{2}\int_0^x \beta(x-\epsilon,\epsilon)\sum_{m=1}^{\infty}\sum_{i=0}^{m-1} v_i(t,x-\epsilon)v_{m-1-i}(t,\epsilon)\mathrm{d}\epsilon\\ &\quad + \sum_{m=1}^{\infty}\sum_{i=0}^{m-1} v_i(t,x)\int_0^{\infty}\beta(x,\epsilon)v_{m-1-i}(t,\epsilon)\mathrm{d}\epsilon\\ &\quad - \int_x^{\infty} b(x|y)s(y)\sum_{m=1}^{\infty} v_{m-1}(t,x)\mathrm{d}y + s(x)\sum_{m=1}^{\infty} v_{m-1}(t,x).\end{aligned}$$

Changing the order of the sums and the substituting $j = m-1-i$, we get

$$\begin{aligned}\sum_{m=1}^{\infty}\mathcal{R}_m\left[\vec{v}_{m-1}\right] &= \sum_{m=1}^{\infty}\frac{\partial v_{m-1}(t,x)}{\partial t} - \frac{1}{2}\int_0^x \beta(x-\epsilon,\epsilon)\sum_{i=0}^{\infty}\sum_{m=i+1}^{\infty} n_i(t,x-\epsilon)v_{m-1-i}(t,\epsilon)\mathrm{d}\epsilon\\ &\quad + \sum_{i=0}^{\infty}\sum_{m=i+1}^{\infty} v_i(t,x)\int_0^{\infty}\beta(x,\epsilon)v_{m-1-i}(t,\epsilon)\mathrm{d}\epsilon\\ &\quad - \int_x^{\infty} b(x|y)s(y)\sum_{m=0}^{\infty} v_m(t,x)\mathrm{d}y + s(x)\sum_{m=0}^{\infty} v_m(t,x)\\ &= \sum_{m=1}^{\infty}\frac{\partial v_{m-1}(t,x)}{\partial t} - \frac{1}{2}\int_0^x \beta(x-\epsilon,\epsilon)\sum_{i=0}^{\infty} v_i(t,x-\epsilon)\sum_{j=0}^{\infty} v_j(t,\epsilon)\mathrm{d}\epsilon\\ &\quad + \sum_{i=0}^{\infty} v_i(t,x)\int_0^{\infty}\beta(x,\epsilon)\sum_{j=0}^{\infty} v_j(t,\epsilon)\mathrm{d}\epsilon\\ &\quad - \int_x^{\infty} b(x|y)s(y)\sum_{m=0}^{\infty} v_m(t,x)\mathrm{d}y + s(x)\sum_{m=0}^{\infty} v_m(t,x).\end{aligned}$$

Combining (2.18) and (2.19), we have

$$\begin{aligned}\frac{\partial n(t,x)}{\partial t} =& \frac{1}{2}\int_0^x \beta(x-\epsilon,\epsilon)n(t,x-\epsilon)n(t,\epsilon)\mathrm{d}\epsilon - n(t,x)\int_0^{\infty}\beta(x,\epsilon)n(t,\epsilon)\mathrm{d}\epsilon\\ &+ \int_x^{\infty} b(x|y)s(y)n(t,y)\mathrm{d}y - s(x)n(t,x).\end{aligned} \tag{2.20}$$

Now, from the initial conditions of $v_m(t,x)$, it holds that

$$n(0,x) = \sum_{m=0}^{\infty} v_m(0,x) = v_0(0,x) + \sum_{m=1}^{\infty} v_m(0,x) = v_0(0,x) = v(0,x).$$

Hence, from the last two expressions, one can observe that $v(t,x)$ must be the exact solution of (1.1). □

3 | NUMERICAL EXAMPLES: RESULTS AND DISCUSSIONS

In this section, we solve five different PBE models with different empirical kernels using homotopy analysis and HPMs. Two problems on pure fragmentation, two problems on pure aggregation, and one problem on simultaneous AF equation are discussed with increasing difficulty level. For choosing these problems, the physical motivation has been discussed in Section 1.2 in detail. Pure fragmentation is linear in nature, whereas aggregation is nonlinear. Note that we are able to present the nth-order general term in the HAM-based series solution of the fragmentation problems for the first time in the literature. This helps to represent the solution in closed form. Thus, suitable choices of the free-to-choose parameters $\hbar$, $H(x)$, $v_0(t,x)$ and then passing the limit, we can generate the exact solution of the corresponding problems. However, due to highly nonlinear nature of the aggregation equations, we are unable to write the series solution in closed form. To overcome this difficulty, we find the first few terms of the series solution and thus generate the semi-analytical solutions for the aggregation models. The HAM-based recursive solution is recalled from Section 2, and the HPM-based recursive solution is recalled from the article.[36] For convenience, we denote the mth-order HPM-based solution as $\hat{c}^{[m]}$. In this context, the HPM-based solution for the simultaneous AF model is not available in the literature. Therefore, we briefly present the recursive scheme and the corresponding HPM-based solution for a smooth study of the readers.

The accuracy of the methods is analyzed over their ability to predict the exact solutions as well as significant moments of different orders. Both qualitative and quantitative analyses of different quantities are presented for all the problems. In order to calculate the error, for a fixed t, we consider the computational domain $\Lambda := [0, 100]$ is divided into I number of subintervals Λ_i. Let x_i and Δx_i denote the midpoint and the length of each subinterval Λ_i. Under these considerations, the error is calculated as follows:[35]

$$\text{Error} := \sum_{i=1}^{I} \left| n(t,x_i) - \hat{v}^{[m]}(t,x_i) \right| \Delta x_i. \tag{3.1}$$

Here, $n(t,x_i)$ and $\hat{v}^{[m]}(t,x_i)$ are the exact solution and mth-order recursive scheme-based solution evaluated at (t,x_i), respectively.

The error for the moments is calculated by using the formula

$$\text{Moment Error} := \left| \mu_i^{exact} - \mu_i^{num} \right|. \tag{3.2}$$

Here, μ_i^{exact} and μ_i^{num} are the exact and recursive scheme-based moments of ith order.

Throughout the computation, we consider $H(t,s) = 1$ in Equation (2.13), and all the required quantities are made dimensionless by scaling them with their initial values. All the computations are executed in a HP Z6 G4 workstation using Mathematica 12.3 software.

3.1 | Pure fragmentation

We consider the pure fragmentation problem with two different selection rates. Table 1 represents the choices of kernels, initial data along with their exact solutions. The exact solutions of the problems are collected from Ziff and McGrady.[25]

Example 3.1. We choose the kernels $b(x|y) = 2/y$, $s(x) = x$ and initial condition $n(0,x) = \exp(-x)$. The exact solution for this problem is given in Table 1.

Putting the values of $b(x|y)$, $s(x)$, and initial condition, the reduced $\mathcal{R}_m$ (2.16) is given by

$$\mathcal{R}_m\left(\vec{v}_{m-1}, t, x\right) = \frac{\partial v_{m-1}(t,x)}{\partial t} - 2\int_x^{\infty} v_{m-1}(t,x)\mathrm{d}y + x v_{m-1}(t,x). \tag{3.3}$$

TABLE 1 Exact solutions for pure fragmentation problems.

S. no.	$b(x\|y)$	$s(x)$	$n(0,x)$	Exact solution
1	$2/y$	x	$\exp(-x)$	$(1+t)^2 \exp[-(1+t)x]$
2	$2/y$	x^2	$\exp(-x)$	$[1+2t(1+x)]^2 \exp\left[-tx^2 - x\right]$

Using the recursive scheme (3.3) along with

$$v_m(t,x) = \chi_m v_{m-1}(t,x) + \int_0^t \hbar H(t,s)\mathcal{R}_m\left(\vec{v}_{m-1},s,x\right) \mathrm{d}s,$$

we obtain

$$\begin{aligned} v_0(t,x) &= \exp(-x), \\ v_1(t,x) &= \exp(-x)\hbar t\,(-2+x)\,, \\ v_2(t,x) &= \frac{1}{2!}\exp(-x)\hbar t\left[2(1+\hbar)(-2+x)+\hbar t\left(2-4x+x^2\right)\right]. \end{aligned}$$

Following the above pattern, the generalized mth term $v_m(t,x)$ for $m \geq 1$ is written as follows:

$$v_m(t,x) = \frac{1}{m!}\exp(-x)\hbar t \sum_{i=1}^{m} L(m,i)\hbar^{i-1}(1+\hbar)^{m-i}\left[i(i-1)-2ix+x^2\right]t^{i-1}x^{i-2}, \tag{3.4}$$

where $L(m,i)$ is the well-known Lah number and is defined by $L(m,i) := \binom{m-1}{i-1}\frac{m!}{i!}$.

The freedom to choose $\hbar$ motivates us to search for a set of values of $\hbar$ for which the HAM-based solution converges rapidly to the exact solution. In this regard, the fifth-order approximation $\hat{v}^{[5]}$ at $t = 1$ and $x = 0.5$ is plotted against $\hbar$ in Figure 1A. It is observed that the graph is flat near -1.75 and in between $[-1,-0.5]$. Thus, method is expected to

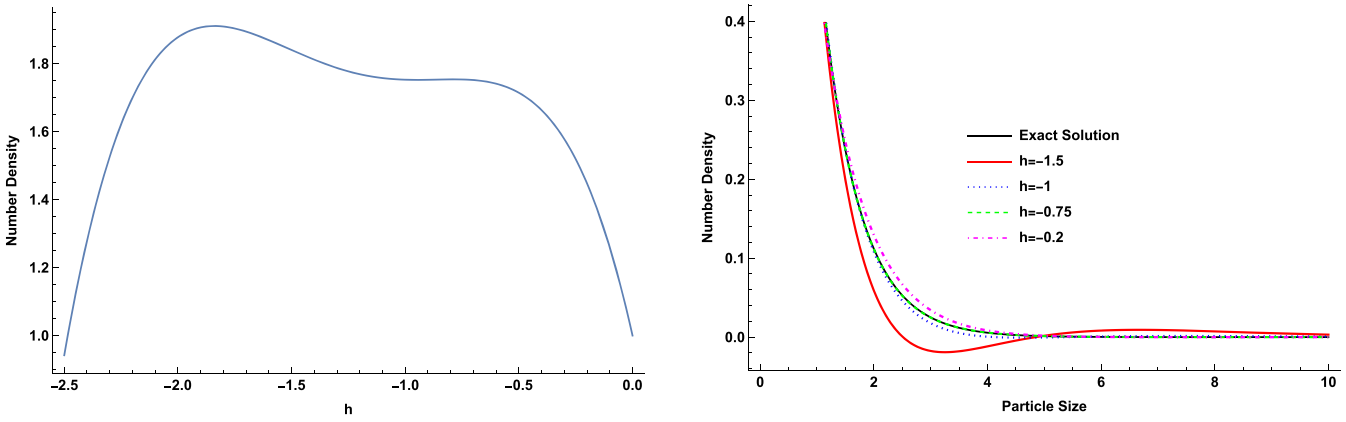

(A) $\hbar$ curve (B) $\hat{v}^{[5]}$ for different values of $\hbar$

FIGURE 1 (A, B) $\hbar$ against $\hat{v}^{[5]}$ for $t = 1$ and $x = 0.5$ for Example 3.1 [Colour figure can be viewed at wileyonlinelibrary.com]

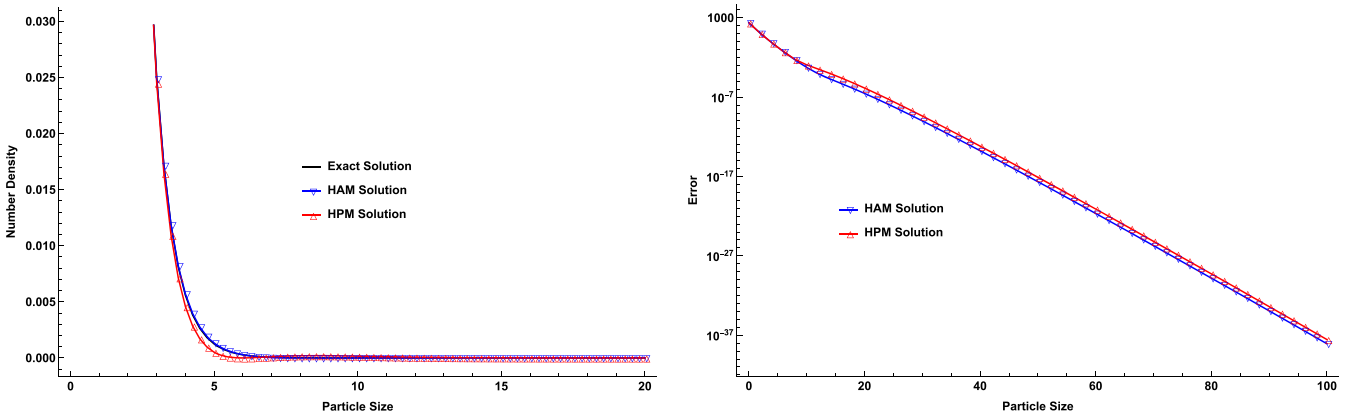

(A) Number density (B) Error graph

FIGURE 2 (A) Number density and (B) error curves for Example 3.1 [Colour figure can be viewed at wileyonlinelibrary.com]

converge rapidly when $\hbar$ lies in the above intervals. We next analyze the HAM-based solution $\hat{v}^{[5]}$ for different values of $\hbar$ in $[-2, -0.2]$. Computing several graphs in Figure 1B, it is observed that $\hat{v}^{[5]}$ is in good agrement with the exact solution for $\hbar = -0.75$.

We now plot $\hat{v}^{[5]}$ and $\hat{c}^{[5]}$ against their exact values in Figure 2A. On the other hand, Figure 2B represents the error graph while plotting the solution. The quantitative error analysis of the solution for the two methods is presented in Table 2.

The above data show that the HAM produces accurate solutions as compared with HPM over coarser grids. As expected due to linear selection rate, the accuracy for both the methods becomes comparable when the number of grid points increases. In the following part, we analyze the methods to predict different significant moment functions. The qualitative comparison is presented in Figure 3, and the quantitative error analysis is presented in Table 3. From Figure 3A and Table 3, we can observe that the zeroth and the first moment are in excellent agreement with exact solution and has minimal error. Figure 3B shows that HAM predicts second-order moment more precisely than HPM method over the considered time duration. The same can be observed from the error in Table 3 as well.

From the above illustrations, it is observed that considering only a five-term solution, HAM exhibits highly accurate results over HPM to predict different quantities.

Example 3.2. Consider the kernels $b(x|y) = 2/y$, $s(x) = x^2$ and initial condition is $n(0, x) = \exp(-x)$.

Setting the above kernels, the recursive scheme (2.16) is written as

$$\mathcal{R}_m\left(\vec{v}_{m-1}, t, x\right) = \frac{\partial v_{m-1}(t,x)}{\partial t} - 2\int_x^\infty x v_{m-1}(t,x)\mathrm{d}y + x^2 v_{m-1}(t,x), \tag{3.5}$$

TABLE 2 Error table for Example 3.1

I	10	20	30	40
Error (HPM)	1.171×10^{-3}	1.414×10^{-6}	4.188×10^{-10}	6.783×10^{-14}
Error (HAM)	5.505×10^{-4}	2.988×10^{-7}	1.025×10^{-10}	1.783×10^{-14}

Abbreviations: HAM, homotopy analysis method; HPM, homotopy perturbation method.

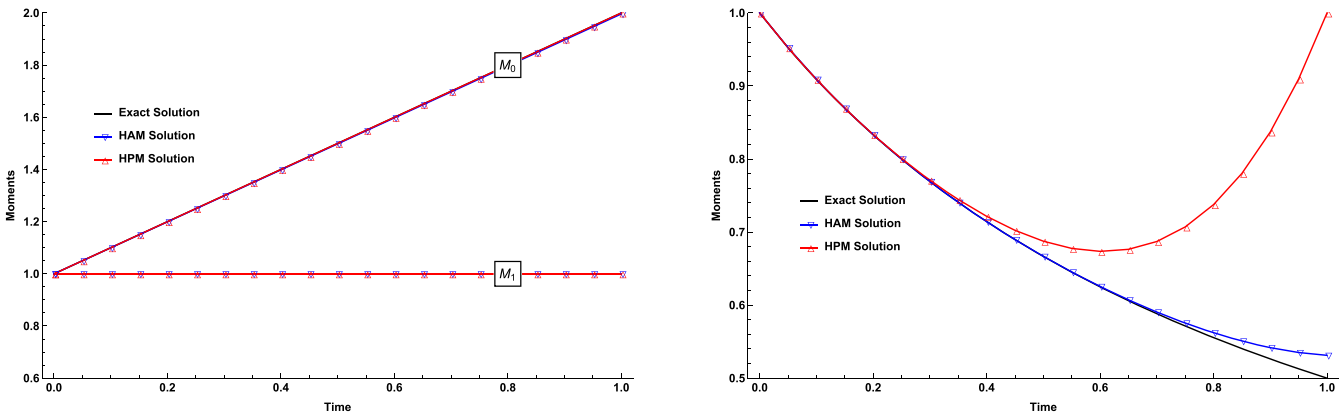

(A) Zeroth and First Moment (B) Second Moment

FIGURE 3 (A, B) Comparison of different moments for Example 3.1 [Colour figure can be viewed at wileyonlinelibrary.com]

TABLE 3 Error analysis of the moments at different times for the Example 3.1

	HAM			HPM		
t	$\mu_0(t)$	$\mu_1(t)$	$\mu_2(t)$	$\mu_0(t)$	$\mu_1(t)$	$\mu_2(t)$
0.2	7.813E-16	0	3.333E-5	0	0	5.333E-4
0.4	1.563E-16	2.220E-16	3.571E-6	6.661E-16	0	0.015
0.6	2.344E-16	0	0.001	3.331E-16	6.661E-16	0.097
0.8	3.125E-16	2.220E-16	0.013	1.776E-16	8.882E-15	0.364
1.0	3.906E-16	0	0.063	8.882E-16	0	1

Abbreviations: HAM, homotopy analysis method; HPM, homotopy perturbation method.

and recalling Equation (2.13)

$$v_m(t,x) = \chi_m v_{m-1}(t,x) + \int_0^t \hbar H(t,s)\mathcal{R}_m\left(\vec{v}_{m-1}, s, x\right) \mathrm{d}s,$$

few initial terms of the HAM-based series solution are calculated as

$$\begin{aligned} v_0(t,x) &= \exp(-x), \\ v_1(t,x) &= \exp(-x)\hbar t\left(-2-2x+x^2\right), \\ v_2(t,x) &= \frac{1}{2!}\exp(-x)\hbar t\left[2(1+\hbar)\left(-2-2x+x^2\right)+\hbar t x^2\left(-4-4x+x^2\right)\right]. \end{aligned}$$

Following the above pattern, we write the generalized $v_m(t,x)$ for $m \geq 1$ as

$$v_m(t,x) = \frac{1}{m!}\exp(-x)\hbar t \sum_{i=1}^{m} L(m,i)\hbar^{i-1}(1+\hbar)^{m-i}\left[-2i-2ix+x^2\right] t^{i-1}x^{2(i-2)}, \tag{3.6}$$

where $L(m,i) := \binom{m-1}{i-1}\frac{m!}{i!}$.

Like the previous example, $\hbar$ is plotted against $\hat{v}^{[5]}$ at $t = 1$ and $x = 0.5$ in Figure 4 to search the suitable range of $\hbar$ for which the HAM-based solution converges rapidly to the exact solution. It is observed that the graph is flat when $\hbar \in [-1.5, -0.25]$.

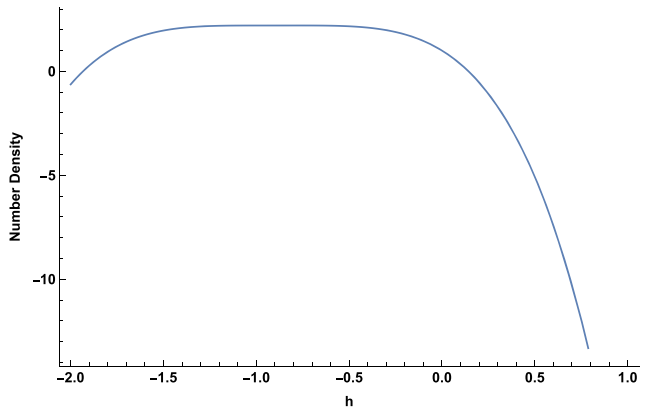

FIGURE 4 $\hbar$ against $\hat{v}^{[5]}$ for $t = 1$ and $x = 0.5$ for Example 3.2 [Colour figure can be viewed at wileyonlinelibrary.com]

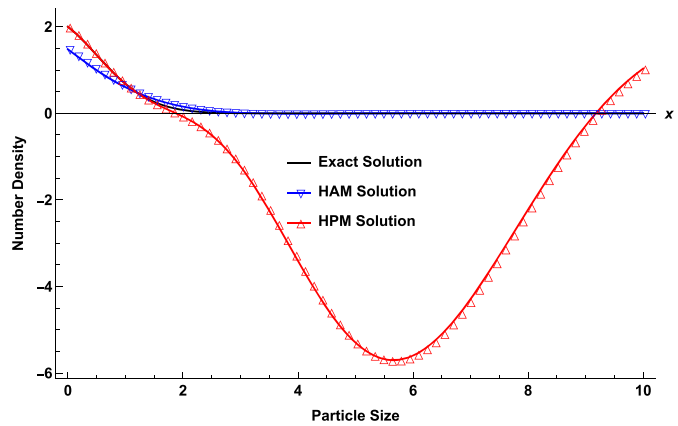

(A) Number density

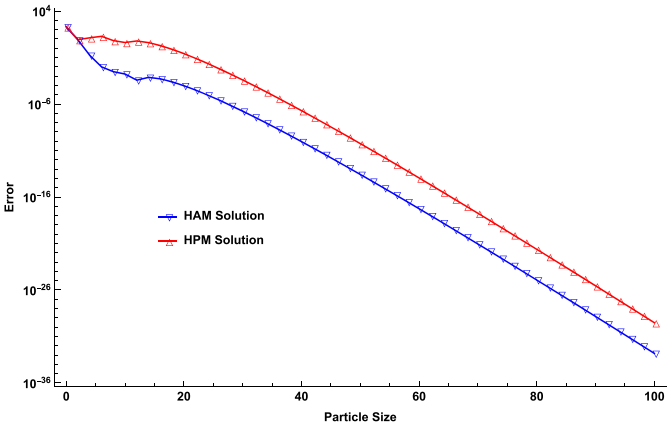

(B) Error graph

FIGURE 5 (A) Number density and (B) error curves for Example 3.2 [Colour figure can be viewed at wileyonlinelibrary.com]

TABLE 4 Error table for Example 3.2.

I	10	20	30	40
Error (HPM)	4.144	0.264	3.872×10^{-4}	1.932×10^{-7}
Error (HAM)	1.679×10^{-3}	9.347×10^{-5}	1.703×10^{-7}	9.067×10^{-11}

Abbreviations: HAM, homotopy analysis method; HPM, homotopy perturbation method.

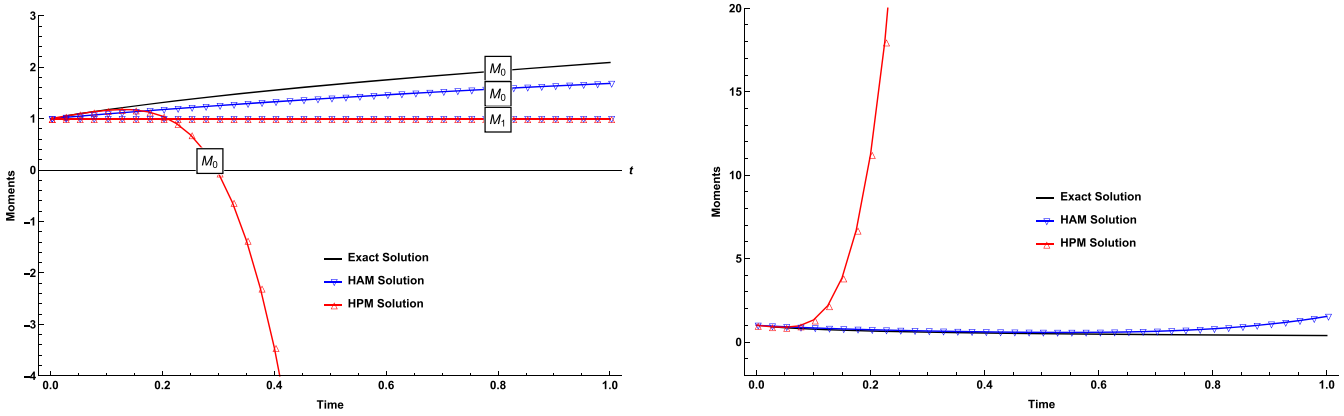

(A) Zeroth and First Moment (B) Second Moment

FIGURE 6 (A, B) Comparison of different moments for Example 3.2 [Colour figure can be viewed at wileyonlinelibrary.com]

TABLE 5 Error analysis of moments at different times for the Example 3.2

	HAM			HPM		
t	$\mu_0(t)$	$\mu_1(t)$	$\mu_2(t)$	$\mu_0(t)$	$\mu_1(t)$	$\mu_2(t)$
0.2	0.139	2.220E-16	0.153	0.267	1.221E-15	21.161
0.4	0.224	2.220E-16	0.136	4.990	1.310E-14	377.82
0.6	0.290	4.441E-16	0.224	26.912	0	1992.1
0.8	0.348	1.332E-15	0.739	87.906	3.064E-14	6430.6
1.0	0.407	5.551E-16	2.291	219.091	0	15905.2

Abbreviations: HAM, homotopy analysis method; HPM, homotopy perturbation method.

In this regard, computing $\hat{v}^{[5]}$ for different values of $\hbar$, it is observed that for $\hbar = -0.65$, the solution $\hat{v}^{[5]}$ shows very good agreement with the exact solution. The qualitative and quantitative analyses of the two methods to predict the solution are studied through Figure 5 and Table 4, respectively. It is evident from Table 4 that even when there are 10 grid points, HAM gives highly precise prediction, whereas HPM has accumulates error heavily. As we increase the number of grids, the error for HAM decreases more rapidly than HPM method. The following results support that HAM predicts the solution with high accuracy even for a small number of approximate terms.

Furthermore, significant moment functions of different orders are plotted in Figure 6, and their error analysis is calculated in Table 5. From Figure 6A, we can observe that the zeroth predicted by HPM is not as accurate as HAM, whereas both methods conserve mass. Figure 6B shows that HPM gives very poor results for second moment as compared with HAM. The error analysis of moments presented in Table 5 supports the above-stated observations from the figures.

The five-term HAM- and HPM-based solutions are compared with respect to the exact values. The HAM-based solutions give more accurate results as compared with the HPM-based solutions.

3.2 | Pure aggregation

We consider the pure aggregation equation with two different sets of kernels. The analytical solutions for the considered problems are collected from Hulburt and Katz[24] and are given in Table 6 below:
where $T(t) = 1 - \exp(-t)$ and $I_1(\cdot)$ is the Bessel function of first kind.

Example 3.3. Consider the kernel $\beta(x,\epsilon) = x + \epsilon$ and initial condition $n(0,x) = \exp(-x)$.

The HAM-based recursive scheme (2.17) is written as

$$\begin{aligned}\mathcal{R}_m\left(\vec{v}_{m-1},t,x\right) =& \frac{\partial v_{m-1}(t,x)}{\partial t} - \frac{1}{2}\int_0^x x\sum_{i=0}^{m-1} v_i(t,x-\epsilon)v_{m-1-i}(t,\epsilon)\mathrm{d}\epsilon \\ &+ \sum_{i=0}^{m-1} v_i(t,x)\int_0^\infty (x+\epsilon)v_{m-1-i}(t,\epsilon)\mathrm{d}\epsilon,\end{aligned} \tag{3.7}$$

and the HAM-based solution is obtained by using the recursive scheme (3.7) along with

$$v_m(t,x) = \chi_m v_{m-1}(t,x) + \int_0^t \hbar H(t,s)\mathcal{R}_m\left(\vec{v}_{m-1},s,x\right)\mathrm{d}s.$$

The first few terms of the series are calculated as follows:

$$\begin{aligned} v_0(t,x) &= \exp(-x),\\ v_1(t,x) &= -\frac{1}{2!}\exp(-x)\hbar t\left(-2-2x+x^2\right),\\ v_2(t,x) &= \frac{1}{2(3!)}\exp(-x)\hbar t\left[-6(1+\hbar)\left(-2-2x+x^2\right)+\hbar t\left(6+18x-3x^2-6x^3+x^4\right)\right].\end{aligned}$$

Like before, $\hat{v}^{[5]}$ is plotted against $\hbar$ in Figure 7 at $t = 1$ and $x = 0.5$. It is observed that the $\hbar-$ curve is flat in $[-0.7,-0.6]$. Therefore, the method is expected to converge rapidly for a value near these points.

Computing number density graphs for different values of $\hbar$, it is observed from Figure 8A that the solution obtained for $h = -0.65$ predicts the number density with high accuracy. Moreover, the error analysis presented in Figure 8B and Table 7 confirms that five-term HAM produces more accurate results than HPM.

Now different moment functions are plotted against their exact values in Figure 9. The error analysis corresponding to different moment functions is given in Table 8. Like before, the HAM-based solution predicts the moments with high accuracy.

Example 3.4. Consider the kernel $\beta(x,\epsilon) = x\epsilon$ and initial condition $n(0,x) = \exp(-x)$.

S. no.	$\beta(x,\epsilon)$	$n(0,x)$	Exact solution
1	$x+\epsilon$	$\exp(-x)$	$\frac{[1-T(t)]\exp[-x(T(t)+1)]I_1\left(2x\sqrt{T(t)}\right)}{x\sqrt{T(t)}}$
2	$x\epsilon$	$\exp(-x)$	$\exp\left[-(t+1)x\right]\sum_{k=0}^{\infty}\frac{t^k x^{3k}}{(k+1)!\Gamma(2k+2)}$

TABLE 6 Exact solutions for pure aggregation problems.

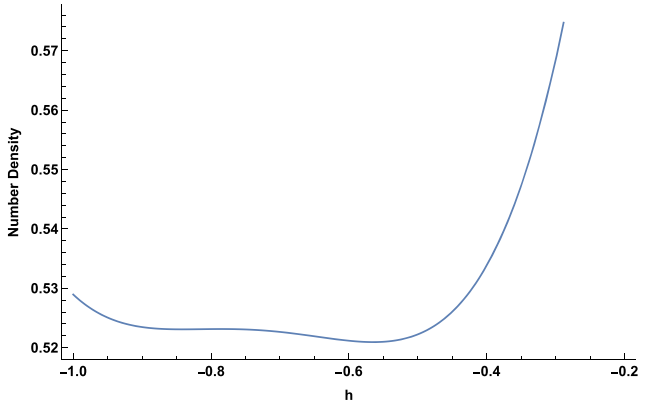

FIGURE 7 $\hbar$ against $\hat{v}^{[5]}$ for $t = 1$ and $x = 0.5$ for Example 3.3 [Colour figure can be viewed at wileyonlinelibrary.com]

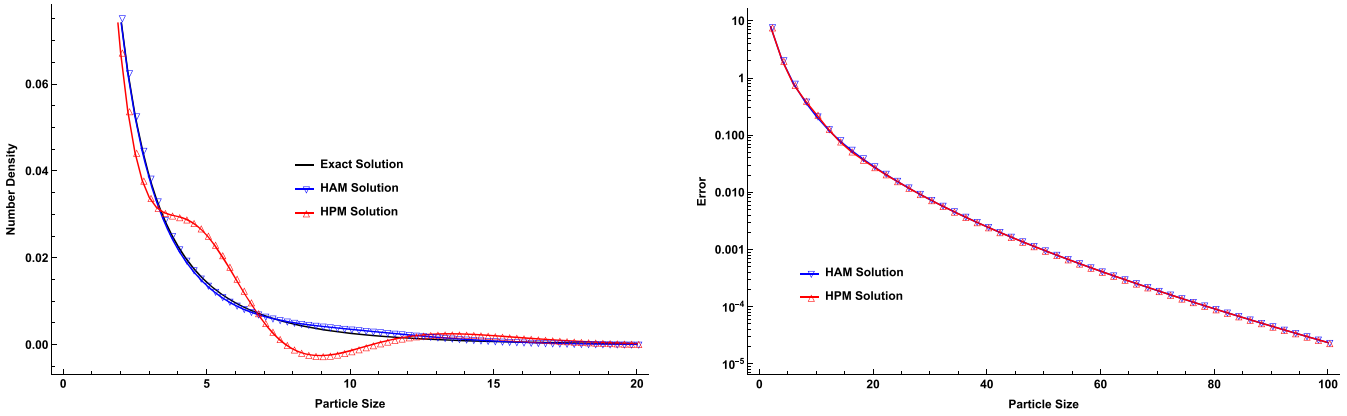

(A) Number density (B) Error graph

FIGURE 8 (A) Number density and (B) error curves for Example 3.3 [Colour figure can be viewed at wileyonlinelibrary.com]

TABLE 7 Error table for Example 3.3.

I	10	20	40	80
Error (HPM)	0.233	0.0282	2.504×10^{-3}	9.193×10^{-5}
Error (HAM)	0.215	0.0279	2.504×10^{-3}	9.192×10^{-5}

Abbreviations: HAM, homotopy analysis method; HPM, homotopy perturbation method.

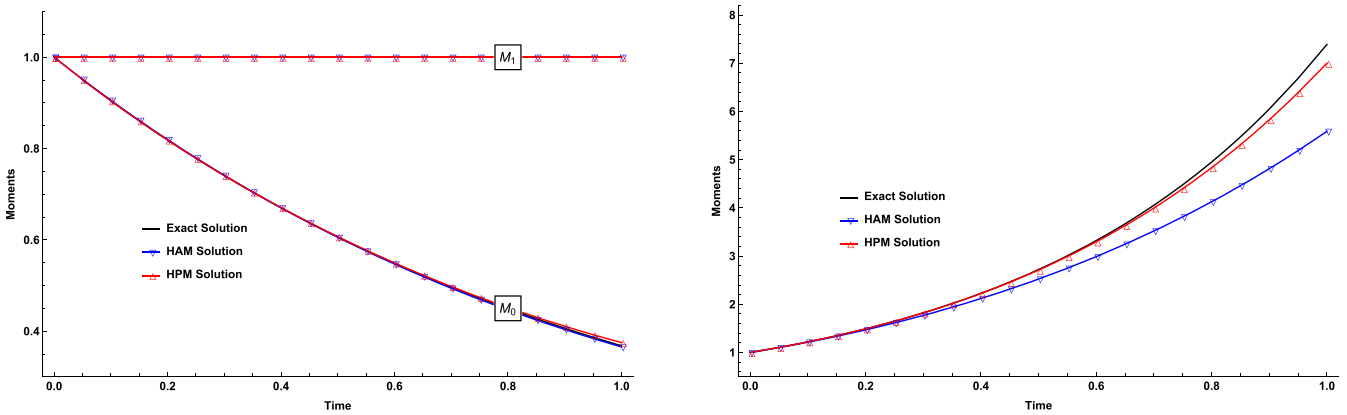

(A) Zeroth and First Moment (B) Second Moment

FIGURE 9 (A, B) Comparison of different moments for Example 3.3 [Colour figure can be viewed at wileyonlinelibrary.com]

TABLE 8 Error for the moments at different times for the Example 3.3.

	HAM			HPM		
t	$\mu_0(t)$	$\mu_1(t)$	$\mu_2(t)$	$\mu_0(t)$	$\mu_1(t)$	$\mu_2(t)$
0.2	2.138E-6	2.220E-16	0.0435	2.580E-6	2.220E-16	1.827E-4
0.4	2.508E-5	0	0.2138	7.995E-5	3.331E-16	0.006
0.6	1.878E-4	8.882E-16	0.6632	5.884E-4	2.220E-16	0.051
0.8	2.793E-3	1.776E-15	1.6517	2.404E-3	4.663E-16	0.235
1.0	2.506E-3	5.773E-15	3.6047	7.121E-3	0	0.778

Abbreviations: HAM, homotopy analysis method; HPM, homotopy perturbation method.

The HAM-based recursive scheme (2.17) reads as

$$\mathcal{R}_m\left(\vec{v}_{m-1}, t, x\right) = \frac{\partial v_{m-1}(t,x)}{\partial t} - \frac{1}{2}\int_0^x (x-\epsilon)\epsilon \sum_{i=0}^{m-1} v_i(t, x-\epsilon) v_{m-1-i}(t,\epsilon)\mathrm{d}\epsilon + \sum_{i=0}^{m-1} v_i(t,x)\int_0^\infty x\epsilon v_{m-1-i}(t,\epsilon)\mathrm{d}\epsilon, \tag{3.8}$$

with

$$v_m(t,x) = \chi_m v_{m-1}(t,x) + \int_0^t \hbar H(t,s)\mathcal{R}_m\left(\vec{v}_{m-1}, s, x\right) \mathrm{d}s,$$

and the first few terms of the HAM-based solution is written as

$$\begin{aligned} v_0(t,x) &= \exp(-x), \\ v_1(t,x) &= -\frac{1}{12}\exp(-x)\hbar t x\left[-12 + x^2\right], \\ v_2(t,x) &= \frac{1}{720}\exp(-x)\hbar t x\left[-60(1+\hbar)(-12+x^2) + \hbar t x(360 - 60x^2 + x^4)\right]. \end{aligned}$$

The following Figure 10 shows that $\hbar-$ curve is parallel to horizontal axis for $\hbar \in [-1, -0.8]$. So, HAM-based solution will converge for some point near these values.

Following the previous methodology, we obtain that HAM-based solutions converge rapidly for $\hbar = -0.775$. Note that $\beta(x,\epsilon) = x\epsilon$ exhibits gelling behavior; that is, infinite size clusters are formed in a finite time-span.[40] Thus, the index (degree) of aggregation is defined as $I_{agg} = 1 - \frac{\mu_0(t)}{\mu_0 0}$, which is a dimensionless form of the zeroth moment and defines the time at which gelation onsets. As mentioned in Kumar et al,[40] we consider $I_{agg}^{gel} = 0.20$ and thus obtain that mass loss occurs at $t = 0.4$. Therefore, the final computation time for this case is taken until $t = 0.4$. Pictorial representation of the number density and the error graph is given in Figure 11, and the corresponding error analysis is presented in Table 9. The figure and table together validate the accuracy of the method.

The moment functions are plotted in Figure 12, and their error analysis is given in Table 10. Both the methods conserve mass until the onset of gelation. HPM produces a poor prediction of the zeroth and second moment. On the other hand, zeroth moment predicted by HAM is in good agrement with exact value, whereas the prediction of second moment is

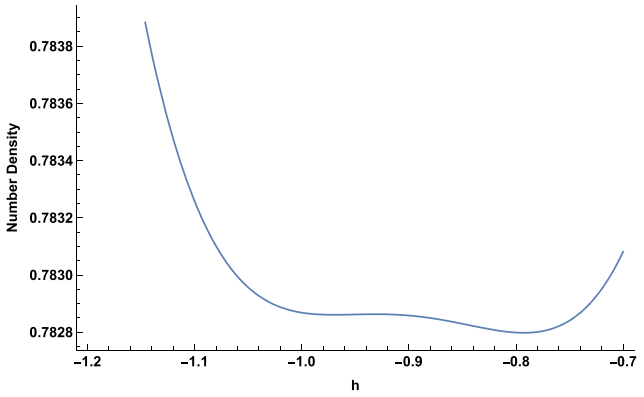

FIGURE 10 $\hbar$ against $\hat{v}^{[5]}$ for $t = 1$ and $x = 0.5$ for Example 3.4 [Colour figure can be viewed at wileyonlinelibrary.com]

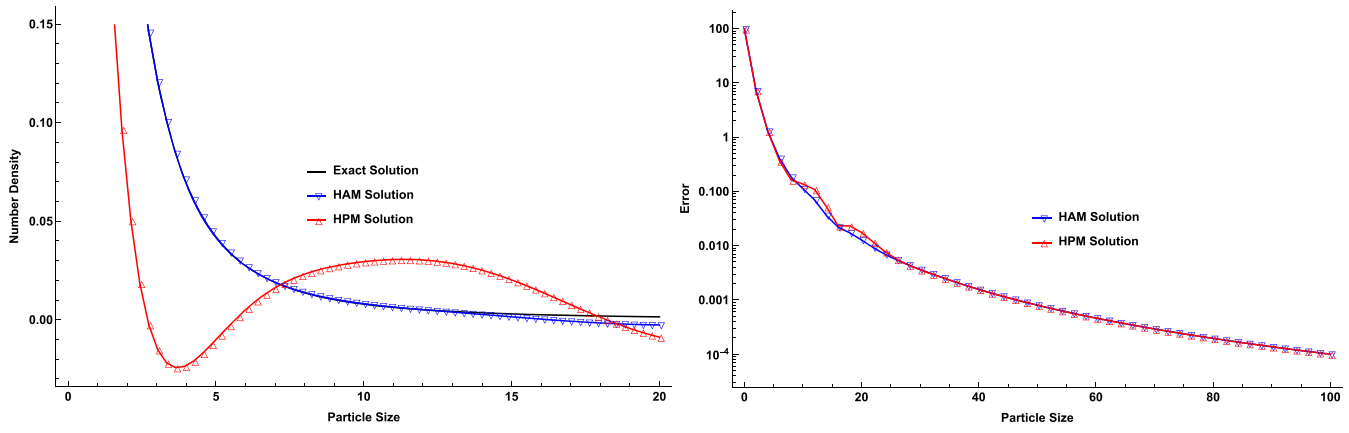

(A) Number density (B) Error graph

FIGURE 11 (A) Number density and (B) error curves for Example 3.4 [Colour figure can be viewed at wileyonlinelibrary.com]

TABLE 9 Error table for Example 3.4

I	10	20	40	80
Error (HPM)	0.137	0.017	1.561×10^{-3}	1.953×10^{-4}
Error (HAM)	0.102	0.012	1.561×10^{-3}	1.952×10^{-4}

Abbreviations: HAM, homotopy analysis method; HPM, homotopy perturbation method.

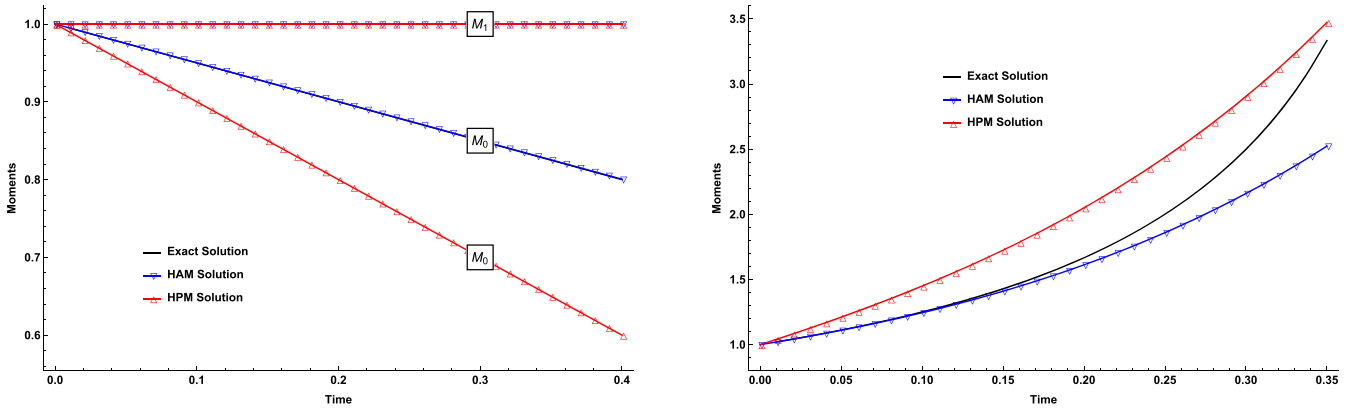

(A) Zeroth and First Moment (B) Second Moment

FIGURE 12 (A, B) Comparison of different moments for Example 3.4 [Colour figure can be viewed at wileyonlinelibrary.com]

TABLE 10 Error analysis of the moments at different times for the Example 3.4

	HAM			HPM		
t	$\mu_0(t)$	$\mu_1(t)$	$\mu_2(t)$	$\mu_0(t)$	$\mu_1(t)$	$\mu_2(t)$
0.1	1.281E-4	7.772E-16	0.010	0.05	8.882E-16	0.399
0.2	2.563E-4	0	0.109	0.10	3.331E-16	0.766
0.3	3.844E-4	2.109E-15	0.680	0.15	1.887E-15	0.811
0.4	5.126E-4	8.882E-16	4.079	0.20	1.665E-15	1.677

Abbreviations: HAM, homotopy analysis method; HPM, homotopy perturbation method.

highly accurate until $t = 0.2$, and it improves with the inclusion of more number of terms in the series solution. The error Table 10 shows that the presented HAM method predicts all three chosen moments precisely as compared with HPM method.

3.3 | Simultaneous AF equation

Example 3.5. We consider the simultaneous AF Equation (1.1) in LPA form as given in McCoy and Madras.[41] The analytical solution is proposed by earlier studies[31,32] for the following set of kernels:

$$\beta(x,\epsilon) = 1,\ S(x) = S_0 x,\ \text{and}\ b(x|y) = 1/y, \tag{3.9}$$

with initial condition $n(0,x) = \exp(-x)$ written as

$$n(t,x) = [\Phi(t)]^2 \exp\left[-x\Phi(t)\right], \tag{3.10}$$

where

$$\Phi(t) := \phi(\infty)\frac{1+\phi(\infty)\tanh\left[\phi(\infty)\frac{t}{2}\right]}{\phi(\infty)+\tanh\left[\phi(\infty)\frac{t}{2}\right]},\ \text{with}\ \phi(\infty) = \sqrt{2S_0}. \tag{3.11}$$

The HPM-based recursive scheme is not available in the literature for this model. Thus, for the convenience of reading, we present the HPM-based recursive scheme for $k \geq 1$ as

$$\begin{aligned}\frac{\partial c_k(t,x)}{\partial t} =& \frac{1}{2}\int_0^x \beta(x-\epsilon,\epsilon)\sum_{i=0}^{k-1} c_i(t,x-\epsilon)c_{k-i-1}(t,\epsilon)\mathrm{d}\epsilon - \sum_{i=0}^{k-1} c_i(t,x)\int_0^\infty \beta(x,\epsilon)c_{k-i-1}(t,\epsilon)\mathrm{d}\epsilon \\ &+ \int_x^\infty b(x|y)c_{k-1}(t,y)s(y)\mathrm{d}y - s(x)c_{k-1}(t,x).\end{aligned} \tag{3.12}$$

Therefore, the HPM-based solution $c_k(t,x)$ is obtained as

$$\begin{aligned}c_0(t,x) &= \exp(-x),\\ c_1(t,x) &= t\left[2S_0 - S_0x - 1 + \frac{x}{2}\right]\exp(-x),\\ c_2(t,x) &= \frac{1}{2}t^2\left[-2S_0 - (2S_0-1)S_0(x-1) + S_0x - S_0x\left(2S_0 - S_0x - 1 + \frac{x}{2}\right)\right.\\ &\quad \left. - \left(S_0 - \frac{1}{2}\right) - \frac{1}{4}(2S_0-1)(x-4)x + 1 - \frac{x}{2}\right]\exp(-x).\end{aligned}$$

We now write the HAM-based recursive scheme (2.15) with kernels (3.9) as

$$\begin{aligned}\mathcal{R}_m\left(\vec{v}_{m-1},t,x\right) =& \frac{\partial v_{m-1}(t,x)}{\partial t} - \frac{1}{2}\int_0^x \sum_{i=0}^{m-1} v_i(t,x-\epsilon)n_{m-1-i}(t,\epsilon)\mathrm{d}\epsilon \\ &+ \sum_{i=0}^{m-1} v_i(t,x)\int_0^\infty v_{m-1-i}(t,\epsilon)\mathrm{d}\epsilon - 2\int_x^\infty S_0 v_{m-1}(t,x)\mathrm{d}y \\ &+ S_0 x v_{m-1}(t,x),\end{aligned} \tag{3.13}$$

and

$$v_m(t,x) = \chi_m v_{m-1}(t,x) + \int_0^t \hbar H(t,s)\mathcal{R}_m\left(\vec{v}_{m-1},s,x\right)\mathrm{d}s. \tag{3.14}$$

Using the recursive scheme (3.13) along with (3.14), we obtain $v_m(t,x)$ for $m \geq 1$ as

$$\begin{aligned}v_0(t,x) &= \exp(-x),\\ v_1(t,x) &= \frac{1}{2}\exp(-x)\hbar t\,(-1+2S_0)\,(-2+x),\\ v_2(t,x) &= \frac{1}{8}\exp(-x)\hbar t\,(-1+2S_0)\left[4(1+\hbar)(-2+x) + \hbar t\left(-6-6x-x^2+2S_0(2-5x+x^2)\right)\right].\end{aligned}$$

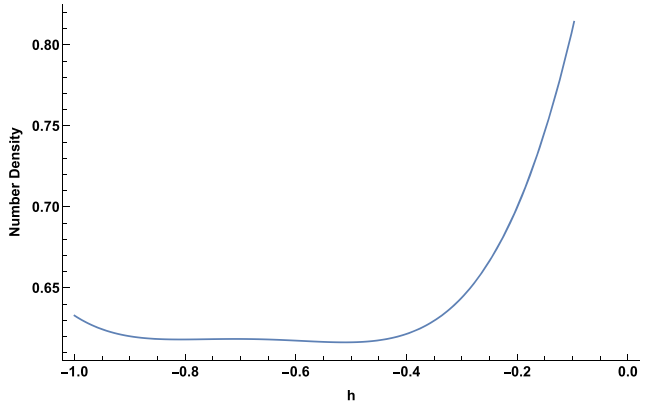

FIGURE 13 $\hbar$ against $\hat{v}^{[5]}$ for $t = 1$ and $x = 0.5$ for Example 3.5 [Colour figure can be viewed at wileyonlinelibrary.com]

Behavior of the solution depends on the value of S_0, that is, on $\phi(\infty) = \frac{\mu_0(t)}{\mu_0(0)} = \sqrt{2S_0}$, which is the ratio of the particle number density at the steady-state condition to its value at the initial condition.[31] Depending upon the value of $\phi(\infty)$, three cases arise: (i) aggregation dominates when $\phi(\infty) < 1$, (ii) fragmentation dominates for $\phi(\infty) > 1$, and (iii) when $\Phi(t) = \phi(\infty) = 1$, the steady-state solution $n(t,x) = \exp(-x) = n(0,x)$ is obtained. In the subsequent discussion, we consider $\phi(\infty) < 1$ by setting $S_0 = 0.1$ which gives $\phi(\infty) = 0.447$.

From Figure 13, we can observe that the $\hbar-$ curve shows flatness in between $[-0.85, -0.45]$.

Computing the graphs for several values of $\hbar$, the best agrement with the exact solution is obtained for $\hbar = -0.725$. We next compute the numerical number density with the particle size distribution and error for both methods. The following results in Figure 14B and Table 11 support that HAM predicts the solution with high accuracy even for a small number of approximate terms.

Figure 15 represents the plots of zeroth-, first-, and second-order moments obtained using HAM and HPM against their exact values.

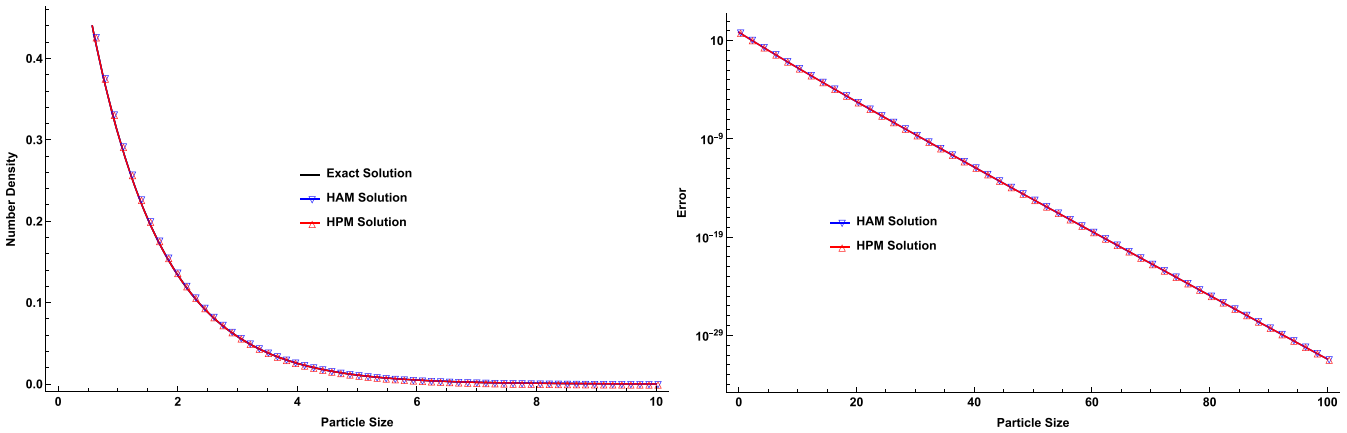

(A) Number density (B) Error graph

FIGURE 14 (A) Number density and (B) error curves for Example 3.5 [Colour figure can be viewed at wileyonlinelibrary.com]

TABLE 11 Error table for Example 3.5

I	10	15	20	25
Error (HPM)	0.0172	3.139×10^{-4}	6.154×10^{-6}	1.276×10^{-7}
Error (HAM)	0.0171	3.133×10^{-4}	6.151×10^{-6}	1.270×10^{-7}

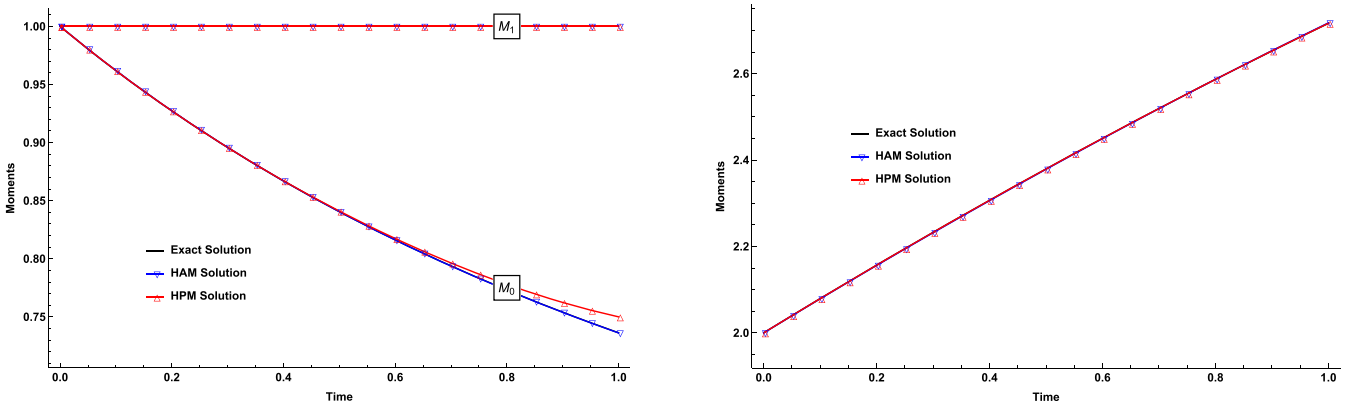

(A) Zeroth and First Moment (B) Second Moment

FIGURE 15 (A, B) Comparison of different moments for Example 3.5 [Colour figure can be viewed at wileyonlinelibrary.com]

Moments obtained from HAM are in good agreement with their exact values. For HPM method, only first- and second-order moments agree with exact solution, and the zeroth moment exhibits overprediction. Error analysis of the moment functions is given in the following table. The data in the Table 12 validate the observations made from the graphs that all the moments are predicted with high accuracy.

Remark 3.1. It can be observed that the graphs of number density and the moments in Examples 3.3 and 3.5 behave in a similar manner. This validates the fact that aggregation dominates whenever $\phi(\infty) < 1$.

Remark 3.2. Setting $S_0 = 2$ implies $\phi(\infty) = 2(> 1)$; that is, when fragmentation dominates, we obtain the following graphs (see Figure 16);

Note that Figures 5 and 6 in Example 3.2 show similar behavior as the above graphs, which validates the fact of fragmentation being dominant for $\phi(\infty) > 1$.

TABLE 12 Error analysis of the moments at different times for the Example 3.5

	HAM			HPM		
t	$\mu_0(t)$	$\mu_1(t)$	$\mu_2(t)$	$\mu_0(t)$	$\mu_1(t)$	$\mu_2(t)$
0.2	1.124E-4	0	1.896E-8	5.895E-6	0	6.929E-4
0.4	7.822E-6	2.220E-16	6.642E-7	1.739E-4	3.331E-16	9.149E-4
0.6	8.236E-5	0	5.458E-6	1.224E-3	1.110E-16	6.623E-4
0.8	1.052E-4	7.772E-16	2.465E-5	0.005	2.220E-16	2.337E-5
1.0	1.106E-4	8.882E-16	7.995E-5	0.014	2.220E-16	1.060E-3

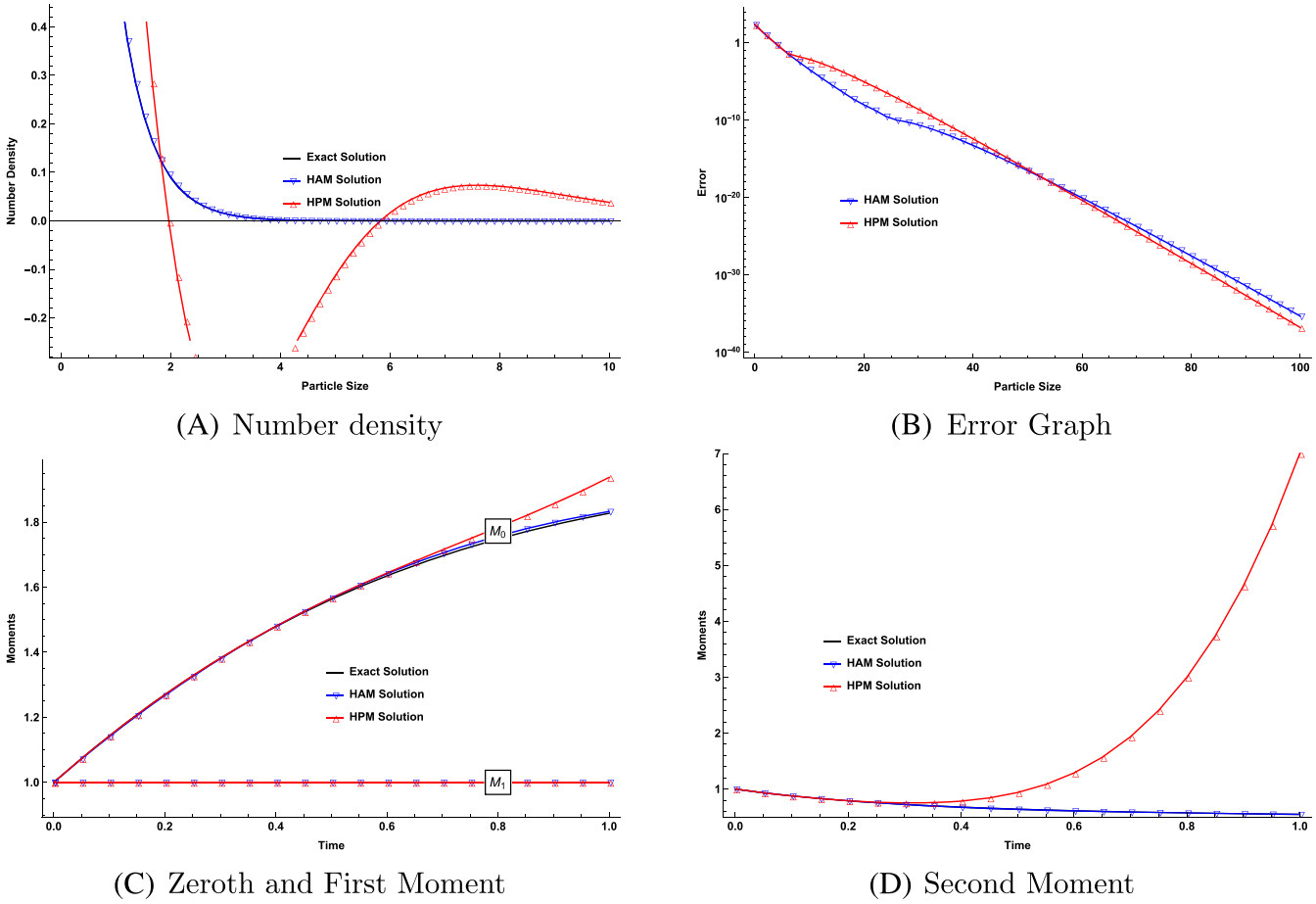

(A) Number density (B) Error Graph

(C) Zeroth and First Moment (D) Second Moment

FIGURE 16 (A–D) Comparison of number density and different moments when $S_0 = 2$ in Example 3.5 [Colour figure can be viewed at wileyonlinelibrary.com]

4 | CONCLUSION

In this paper, the HAM is used to define numerical schemes for solving different kind of PBEs. The method generates series solutions, and the corresponding recursive scheme for the same is obtained. The series solution in closed form is written for fragmentation models. Detailed convergence analysis is also performed for the newly defined recursive scheme. Evaluation of number density along with its different moments is studied, and a detailed error analysis is also carried out and compared with the existing HPM-based solutions. It is observed that the overall agreement of the results by the HAM-based solutions with the analytical solution is better than the HPM-based solutions. Moreover, HPM produces very poor prediction as the size dependency of the model increases.

ACKNOWLEDGEMENT

The authors are thankful to an anonymous reviewer for his/her valuable suggestions, which helped towards the improvement of the manuscript.

CONFLICT OF INTEREST

This work does not have any conflicts of interest.

ORCID

Prakrati Kushwah https://orcid.org/0000-0002-6984-7512
Jitraj Saha https://orcid.org/0000-0002-8864-5537

REFERENCES

1. Dubovski PB. Structural stability of disperse systems and finite nature of a coagulation front. *J Exp Theor Phys*. 1999;89:384-390.
2. Kobayashi H, Tanaka H. Rapid formation of gas-giant planets via collisional coagulation from dust grains to planetary cores. *Astrophys J*. 2021;922:16.
3. Xue Y, Wang L-P, Grabowski Wojciech W. Growth of cloud droplets by turbulent collision–coalescence. *J Atmos Sci*. 2008;65:331-356.
4. Li XY, Brandenburg A, Svensson G, Haugen NE, Mehlig B, Rogachevskii I. Effect of turbulence on collisional growth of cloud droplets. *J Atmos Sci*. 2018;75:3469-3487.
5. Castro JM, Burgisser A, Schipper CI, Mancini S. Mechanisms of bubble coalescence in silicic magmas. *Bull Volcanol*. 2012;74:2339-2352.
6. Mancini S, Forestier-Coste L, Burgisser A, James F, Castro J. An expansion–coalescence model to track gas bubble populations in magmas. *J Volcanol Geotherm Res*. 2016;313:44-58.
7. Robson DT, Annibale A, Baas ACW. Reproducing size distributions of swarms of barchan dunes on Mars and Earth using a mean-field model. *Phys A: Stat Mech Appl*. 2022;2022:128042.
8. Génois M, Hersen P, Bertin E, Du Pont SC, Grégoire G. Out-of-equilibrium stationary states, percolation, and subcritical instabilities in a fully nonconservative system. *Physical Review E*. 2016;94(04):2101.
9. Ahamed F, Singh M, Song HS, Doshi P, Ooi CW, Ho Y. On the use of sectional techniques for the solution of depolymerization population balances. *Results Discret-Contin Mesh Adv Powder Technol*. 2020;31:2669-2679.
10. Shirazian S, Ismail HY, Singh M, Shaikh R, Croker DM, Walker GM. Multi-dimensional population balance modelling of pharmaceutical formulations for continuous twin-screw wet granulation: determination of liquid distribution. *Int J Pharm*. 2019;566:352-360.
11. Bart H-J, Drumm C, Attarakih MM. Process intensification with reactive extraction columns. *Chem Eng Process: Process Intensification*. 2008;47:745-754.
12. Erabit N, Ndoye FT, Alvarez G, Flick D. A population balance model integrating some specificities of the β-lactoglobulin thermally-induced aggregation. *J Food Eng*. 2015;144:66-76.
13. Metzger L, Kind M. The influence of mixing on fast precipitation processes—a coupled 3D CFD-PBE approach using the direct quadrature method of moments (DQMOM). *Chem Eng Sci*. 2017;169:284-298.
14. Ismail HY, Singh M, Albadarin AB, Walker GM. Complete two dimensional population balance modelling of wet granulation in twin screw. *Int J Pharm*. 2020;591:120018.
15. Dürr R, Bück A. Influence of moisture control on activity in continuous fluidized bed drying of baker's yeast pellets. *Drying Technol*. 2020;2020:1-6.
16. Saha J, Kumar J. The singular coagulation equation with multiple fragmentation. *Zeitschrift fü,r angewandte Mathematik und Physik*. 2015;66:919-941.
17. Elminyawi IM, Gangopadhyay S, Sorensen CM. Numerical solutions to the Smoluchowski aggregation–fragmentation equation. *J Colloid Interface Sci*. 1991;144:315-323.
18. McCoy BJ, Madras G. Evolution to similarity solutions for fragmentation and aggregation. *J Colloid Interface Sci*. 1998;201:200-209.

19. Wang L, Marchisio DL, Vigil RD, Fox RO. CFD simulation of aggregation and breakage processes in laminar Taylor–Couette flow. *J Colloid Interface Sci*. 2005;282:380-396.
20. Matveev SA, Stadnichuk VI, Tyrtyshnikov EE, Smirnov AP, Ampilogova NV, Brilliantov NV. Anderson acceleration method of finding steady-state particle size distribution for a wide class of aggregation–fragmentation models. *Comput Phys Commun*. 2018;224:154-163.
21. Frungieri G, Vanni M. Aggregation and breakup of colloidal particle aggregates in shear flow: a combined Monte Carlo-Stokesian dynamics approach. *Powder Technol*. 2021;388:357-370.
22. Shen X, Lin M, Zhu Y, et al. A quasi-Monte Carlo based flocculation model for fine-grained cohesive sediments in aquatic environments. *Water Res*. 2021;194:116953.
23. Wu S, Yang S, Tay KL, Yang W, Jia M. A hybrid sectional moment projection method for discrete population balance dynamics involving inception, growth, coagulation and fragmentation. *Chem Eng Sci*. 2022;249:117333.
24. Hulburt HM, Katz S. Some problems in particle technology: a statistical mechanical formulation. *Chem Eng Sci*. 1964;19:555-574.
25. Ziff RM, McGrady ED. The kinetics of cluster fragmentation and depolymerisation. *J Phys A Math Gen*. 1985;18:3027.
26. Ziff RM. New solutions to the fragmentation equation. *J Phys A Math Gen*. 2821;1991:24.
27. Kumar J, Peglow M, Warnecke G, Heinrich S, Mörl L. Improved accuracy and convergence of discretized population balance for aggregation The cell average technique. *Chem Eng Sci*. 2006;61:3327-3342.
28. Kumar R, Kumar J. Numerical simulation and convergence analysis of a finite volume scheme for solving general breakage population balance equations. *Appl Math Comput*. 2013;219:5140-5151.
29. Kumar R, Kumar J, Warnecke G. Moment preserving finite volume schemes for solving population balance equations incorporating aggregation, breakage, growth and source terms. *Math Models Methods Appl Sci*. 2013;23:1235-1273.
30. Marchisio DL, Fox RO. Solution of population balance equations using the direct quadrature method of moments. *J Aerosol Sci*. 2005;36:43-73.
31. Lage PLC. On the representation of QMOM as a weighted-residual method—the dual-quadrature method of generalized moments. *Compu Chem Eng*. 2011;35:2186-2203.
32. Yuan C, Laurent F, Fox RO. An extended quadrature method of moments for population balance equations. *J Aerosol Sci*. 2012;51:1-23.
33. Robson DT, Baas ACW, Annibale A. A combined model of aggregation, fragmentation, and exchange processes: insights from analytical calculations. *J Stat Mech: Theory Exper*. 2021;2021:53203.
34. Gunawan R, Fusman I, Braatz RD. High resolution algorithms for multidimensional population balance equations. *AIChE J*. 2004;50:2738-2749.
35. Singh R, Saha J, Kumar J. Adomian decomposition method for solving fragmentation and aggregation population balance equations. *J Appl Math Comput*. 2015;48:265-292.
36. Kaur G, Singh R, Singh M, Kumar J, Matsoukas T. Analytical approach for solving population balances: a homotopy perturbation method. *J Phys A Math Theor*. 2019;52:385201.
37. He J-H. Homotopy perturbation method: a new nonlinear analytical technique. *Appl Math Comput*. 2003;135:73-79.
38. Liao S. *Beyond Perturbation Introduction to Homotopy Analysis Method Modern mechanics and mathematics*: CRC Press; 2004.
39. Liao S. Comparison between the homotopy analysis method and homotopy perturbation method. *Appl Math Comput*. 2005;169:1186-1194.
40. Kumar J, Kaur G, Tsotsas E. An accurate and efficient discrete formulation of aggregation population balance equation. *Kinet Related Models*. 2016;9:373.
41. McCoy BJ, Madras G. Analytical solution for a population balance equation with aggregation and fragmentation. *Chem Eng Sci*. 2003;58:3049-3051.

How to cite this article: Kushwah P, Saha J. Improved accuracy and convergence of homotopy-based solutions for aggregation–fragmentation models. *Math Meth Appl Sci*. 2023;46(6):7180-7200. doi:10.1002/mma.8963